

A FINITE-ELEMENT TREATMENT OF SEA ICE DYNAMICS FOR DIFFERENT ICE RHEOLOGIES

R. M. S. M. SCHULKES[†], L. W. MORLAND* AND R. STAROSZCZYK[‡]

School of Mathematics, University of East Anglia, Norwich NR4 7TJ, U.K.

SUMMARY

In this paper the effects of four different rheologies on the evolution of a large-scale sea ice pack are determined and compared. Two rheologies are of viscous-plastic form, and two are viscous fluid relations. The initial pack domain is rectangular, and the motion is driven by wind stress and resisted by ocean drag. Two adjacent edges are rigid shore boundaries, and the other two are free boundaries at open water which move during the pack motion, so that the pack domain changes in time. Two different forms of boundary conditions at the rigid shore edges are considered, which also influence the evolution. The governing equations are solved numerically using a finite-element method, and, unlike previous numerical treatments, no artificial viscosity is incorporated to stabilise the algorithm near interfaces between converging and diverging flow. Instability arises when any tensile stress is abruptly cut-off when diverging flow is initiated, and an alternative view is offered. © 1998 John Wiley & Sons, Ltd.

Int. J. Numer. Anal. Meth. Geomech., Vol. 22, 153–174 (1998)

Key words: finite-element; sea ice pack; rheology; viscous-plastic; viscous fluid

1. INTRODUCTION

The effect of the Polar sea ice masses on the global climate has long been recognized, and a full theory of global climate changes must incorporate the dynamics of the ice covers in the Polar regions. Ultimately, the theory must couple general circulation models of the ocean and the atmosphere to the ice pack dynamics in order to understand and predict the behaviour of the ice cover and the climate. However, the dynamics of the ice cover is extremely complex, and the formulation of a model which just describes the main features of the observed behaviour of the ice cover encounters significant difficulties.

A sea ice pack does not constitute a rigid plate overlying the ocean but, rather, consists of a multitude of floes of vastly different sizes driven by ocean currents, wind stresses and Coriolis forces. The floes move about continuously, breaking and rotating because of inter-floe collisions. As a result of the inter-floe movements large variations in the ice concentration and ice thickness can occur. Of vital importance in relation to oceanographic and atmospheric processes is the ability to predict the large-scale motion of the ice cover together with the ice concentration

* Correspondence to: L. W. Morland, School of Mathematics, University of East Anglia, Norwich NR4 7TJ, U.K.

[†] Now at: Norsk Hydro Research Centre Porsgrunn, P.O. Box 2560, N-3901 Porsgrunn, Norway

[‡] On leave from the Institute of Hydroengineering, Polish Academy of Sciences, ul. Waryńskiego 17, 71-310 Szczecin, Poland

and ice thickness. Significant progress has been made on modelling of sea ice dynamics in polar regions, but there are still various features needing attention. One aspect concerns the evolution equations for the area fraction and the ice thickness. A number of different sets of evolution equations have been employed over the years, the simplest set being that used by Hibler.¹ Implicit in Hibler's evolution equations is the assumption that there is no vertical mass transfer. This assumption leads to the well-known problem that the area fraction A is not bounded above during sustained convergence. The thickness distribution model proposed by Thorndike *et al.*² and recently extended by Flato and Hibler³ overcomes this problem, but at the cost of a significant increase in the computational effort. Shinohara⁴ indicated how the original model by Hibler¹ could be extended by including a ridging function and thereby limiting the increase in the area fraction during sustained convergence. Using the framework of interacting continua, Gray and Morland⁵ have derived a two-dimensional reduced model by depth integration of the full three-dimensional mixture equations, and incorporate a ridging process that correctly restricts the area fraction. Recently it was shown by Schulkes⁶ that with a proper identification of the ridging functions, the thickness distribution model of Thorndike *et al.*² and the models of Shinohara⁴ and Gray and Morland⁵ are, in fact, closely related. However, Gray and Morland⁵ showed that there are inconsistencies between the direct two-dimensional mass and momentum balance formulations given by Hibler,¹ and adopted in continuing applications.

A second aspect of modelling large-scale sea ice covers concerns the constitutive law which describes the behaviour of sea ice on a geophysical scale. Essentially, two classes of constitutive relation have been adopted. The first, the viscous-plastic theory developed by Hibler^{1,7} is derived from a yield curve in the two-dimensional principal stress space with an associated flow rule for high strain rates, and a distinct viscous law for lower strain rates. Various shapes of the yield curve have been proposed ranging from a teardrop shape⁸ and an ellipse,¹ to triangular shapes for the Mohr–Coulomb rheology and lines for the cavitating fluid model.⁹ The second treats the ice cover as a non-linearly viscous fluid, satisfying the two-dimensional restriction of the general Reiner–Rivlin fluid constitutive relation. Smith¹⁰ has proposed six postulates which a constitutive law for sea ice should obey, and constructed a constitutive relation using these postulates. Overland and Pease¹¹ employed Smith's postulates to construct a simple rheology for coastal sea ice. While Smith's postulates give general properties of the constitutive relation, there is still a large degree of freedom in constructing the functions. For this reason it is important to conduct careful numerical studies to determine important features of the different rheologies. A comparison of accurate field data and numerical results should ultimately lead to a realistic rheology.

Many numerical simulations of sea ice motions have been based on Hibler's¹ equations for the dynamics, both for the viscous-plastic and viscous fluid rheologies. Examples of finite-element treatments are Thomson *et al.*,¹² who compare different rheologies, and Thomson and Sykes,¹³ who investigate sensitivity to changes of input assumptions. More common are finite-difference treatments. Examples are Leppäranta and Hibler,¹⁴ who construct a one-dimensional flow simulation to describe a marginal ice zone, and confirm accuracy of the numerical algorithm with a special analytic solution. Ip *et al.*¹⁵ simulate seasonal variations, Flato and Hibler⁹ have compared the behaviour of the viscous-plastic, the cavitating fluid and the Mohr–Coulomb rheologies in an Arctic Basin simulation, and Hibler and Ip¹⁶ construct an Arctic Basin simulation for correlation with buoy drifts. While such simulations give insight into the characteristics of these rheologies, a numerical investigation of a problem which is geometrically much simpler can focus on the model features rather than the consequences of a complex domain. This approach to testing models was adopted by Flato,¹⁷ who investigated the evolution of an ice

cover in a simple rectangular domain where at three of the boundaries the ice cover was constrained, while one boundary was a free water edge. The rheology is likely to have a significant influence on the motion of the free boundary, and inclusion of a free boundary is a necessary ingredient in numerical tests.

All the above treatments follow Hibler's¹ cut-off of tensile stress in diverging flow, and use artificial viscosity to stabilize the numerical algorithm near converging-diverging flow interfaces. However, Gray and Killworth¹⁸ emphasize that this approach must result in solutions which are functions of the fictitious numerical diffusion, and to an uncertain extent. They also demonstrate analytically and numerically the instability of Hibler's¹ model with tensile stress cut-off for a simple one-dimensional problem, and the unsatisfactory neutral stability of the simpler cavitating fluid model^{9,19} for the same problem. Schulkes⁶ confirmed by asymptotic analysis the global stability of the Hibler¹ model, but the analysis of Gray and Killworth¹⁸ shows that a numerical algorithm must become locally unstable so that the solution cannot proceed without distortion. Here we adopt the self-consistent balance equations derived by Gray and Morland,⁵ and do not introduce additional artificial numerical terms. We focus on a simple initial domain, a rectangle, but generalise Flato's¹⁷ problem by having two adjacent sides stress free, at a water edge, and two along rigid shores. On the rigid boundaries both non-slip and free-slip conditions are considered, in conjunction with a bonding condition of zero normal velocity. The motion is driven by a simple uniform wind stress parallel to one shore, resisted by ocean drag. Four different rheologies are considered, two of the viscous plastic form, two of the viscous fluid form, with both types of rigid boundary conditions. A variety of finite-element solutions which compare the influences of the different rheologies described above, and the different rigid boundary conditions, are presented. In particular, one set adopts tensile stress cut-off and confirms the numerical instability, but it is demonstrated also that a viscous-plastic model without cut-off can lead to instabilities for one of the rigid shore boundary conditions. An alternative view to abrupt cut-off is offered, which yields stable solutions. This restriction to a simple geometry and simple forcing allows both the numerical technique and the model features to be assessed, which can be buried in a large-scale simulation of a realistic pack geometry and forcing.

It should be noted that the determination of the moving position of an ice edge is an important problem in its own right. For example, drilling rigs used by the off-shore oil and gas industry in the Bering Sea cannot withstand sea ice forces, and hence, operations must terminate when the ice edge gets too close. In order to avoid excessive risks or loss of revenue due to too early withdrawals, it is clear that the position of the ice edge must be predicted accurately. One of the attempts to determine the position of an ice edge was presented by Pritchard *et al.*,²⁰ who used a combination of a fixed Eulerian grid and a deforming Lagrangian grid to try to improve the ice edge resolution. Flato¹⁷ has implemented the particle-in-cell method to demonstrate its ability to deal with large spatial deformations of an ice edge. The extensive free boundary considered here can be expected to be a more demanding numerical problem, and is, both because it induces a more complex unknown moving domain than in more constrained geometries, and because it can initiate more extensive divergent zones. A reliable numerical algorithm must be able to treat such situations.

2. GOVERNING EQUATIONS

The state of a large-scale sea ice cover is generally described in terms of the ice thickness $h(\mathbf{x}, t)$, the area fraction $A(\mathbf{x}, t)$ (defined to be the fractional ice cover per unit area) and the velocity field

$v_i(\mathbf{x}, t)$, $i = 1, 2$. Furthermore, it is commonly assumed that the motion of the ice cover is entirely in the x_1, x_2 -plane with motion in the vertical direction being neglected. The momentum equations governing the motion of the ice cover are obtained⁵ by integrating the full three-dimensional equation through the thickness of the ice cover,

$$\rho h \frac{D\mathbf{v}}{Dt} = \rho h \left[\frac{\partial \mathbf{v}}{\partial t} + \mathbf{v} \cdot \nabla \mathbf{v} \right] = \nabla \cdot \mathbf{N} + \mathbf{f}_T + \mathbf{f}_B. \quad (1)$$

in which ρ is the constant intrinsic ice density, D/Dt is the material time-derivative convected with the velocity field \mathbf{v} , \mathbf{f}_T , \mathbf{f}_B are the external tractions exerted on the top and the bottom of the ice cover by wind stress and ocean drag, and \mathbf{N} is the depth integrated horizontal stress tensor relative to the local water pressure. For the purpose of this comparison study, a dynamic sea level and Coriolis forces are neglected; they do not change the structure of the system of equations, but the latter must influence the actual flow. A coupled energy balance is also omitted since this study is primarily concerned with the mechanical response of the ice cover.

Movement of the ice cover under the action of ocean currents or wind stress leads to variations in the ice thickness and the area fraction, which are governed by the ice and lead water mass balances and the ridging process. The evolution equations for the ice thickness and the area fraction, obtained by depth integration of the point balances, are, neglecting melt and refreeze at the floe edges and surface and base,⁵

$$\frac{DA}{Dt} + A(1 - \mathcal{R})\nabla \cdot \mathbf{v} = 0 \quad (2)$$

$$\frac{Dh}{Dt} + \mathcal{R}h\nabla \cdot \mathbf{v} = 0 \quad (3)$$

In the above equations $\mathcal{R}(A, h, \dots)$ is a ridging function which may depend on the state variable such as the ice thickness and the area fraction. Both Shinohara⁴ and Gray and Morland⁵ choose \mathcal{R} to be of the form

$$\mathcal{R} = r(A, h)H(-\eta) \quad (4)$$

in which $H(\theta)$ denotes the unit Heaviside function and $\eta = \nabla \cdot \mathbf{v}$ is the first invariant of the rate of strain tensor. This choice of the ridging function ensures that during divergence the ice thickness remains constant and open water is produced, in accordance with the main properties of the thickness distribution model of Thorndike *et al.*² The function $r(A, h)$ is required to satisfy the conditions $A \rightarrow 0$ as $r \rightarrow 0$ and $A \rightarrow 1$ as $r \rightarrow 1$. Gray and Morland⁵ show that with such a ridging function, the area fraction remains bounded within the limits $0 \leq A \leq 1$, as required. Note that Hibler¹ and followers use a partial or mean thickness $\bar{h} = Ah$.

3. RHEOLOGIES

One aim of this paper is to compare the behaviour of the model described by equations (1)–(4) for different constitutive relations. As noted earlier, there are essentially two classes of relations in common use: those derived from a yield curve with associated flow rule and those based on the Reiner–Rivlin fluid law. We choose two from each class. First consider the viscous-plastic (VP) rheology proposed by Hibler.^{1, 7} The viscous relation derived from an associated normal flow rule for an elliptic yield curve in the horizontal principal stress axes (omitting reference to the depth

integration for convenience), with e the ratio of the major to minor axis, is given by

$$N_{ij} = 2\mu D_{ij} + (\zeta - \mu) D_{kk} \delta_{ij} - \frac{P}{2} \delta_{ij} \quad (i, j, k = 1, 2) \quad (5)$$

in which

$$\zeta = \frac{P}{2\Delta}, \quad \mu = \frac{\zeta}{e^2} \quad \text{for } \Delta \geq \Delta_c = 2 \times 10^{-9} \text{ s}^{-1} \quad (6)$$

are functions of a combination Δ of the dilatational and shear strain-rate invariants η and γ :

$$\eta = \nabla \cdot \mathbf{v} = D_{kk}, \quad \gamma^2 = \frac{1}{2} (\hat{D}_{kk})^2, \quad \Delta = (\eta^2 + 4\gamma^2/e^2)^{1/2} \quad (7)$$

and

$$\zeta = \zeta_{\max}, \quad \mu = \mu_{\max} = \zeta_{\max}/e^2 \quad \text{for } \Delta \leq \Delta_c, \quad \text{where } \zeta_{\max} = P/(2\Delta_c) \quad (8)$$

In Hibler^{1,7} ζ and μ were termed the bulk and shear viscosities respectively, but are strictly viscosities multiplied by the thickness in view of the definition of \mathbf{N} . The two-dimensional horizontal strain-rate tensor \mathbf{D} and deviatoric strain-rate tensor $\hat{\mathbf{D}}$ are given by

$$D_{ij} = \frac{1}{2} \left(\frac{\partial v_i}{\partial x_j} + \frac{\partial v_j}{\partial x_i} \right), \quad \hat{D}_{ij} = D_{ij} - \frac{1}{2} \eta \delta_{ij}, \quad (i, j = 1, 2) \quad (9)$$

where δ_{ij} are the components of the two-dimensional unit tensor. This disjoint viscous relation is adopted to avoid unbounded viscosities as strain-rate approaches zero. The term $P = P(A, h)$ is twice the mean pressure predicted by the viscous relation at zero strain-rate, which is described as the ice strength, and is assumed to have the form

$$P(A, h) = P^* h A f(A) = P^* h A e^{-K(1-A)} \quad (10)$$

in which P^* and K are empirical constants. Note that Hibler¹ does not explicitly include the factor A which arises in a consistent definition of \mathbf{N} .

A limiting form of the viscous-plastic rheology is the cavitating-fluid (CF) model. For the cavitating-fluid model the yield curve in principal stress space is simply a straight line along the major axis of the elliptical yield curve of the VP-rheology, Flato and Hibler.⁹ The main characteristics of the CF-rheology are that the ice pack is assumed to have no shear or tensile strength, and supports only isotropic pressure. The zero shear viscosity limit is obtained from the VP-rheology by taking the limit $e \rightarrow \infty$ in (5)–(7), obtaining

$$N_{ij} = \begin{cases} \frac{P}{2} [\text{sgn}(\eta) - 1] \delta_{ij}, & |\eta| > \eta_{\min} \\ \left(\zeta_{\max} \eta - \frac{P}{2} \right) \delta_{ij}, & |\eta| < \eta_{\min} \end{cases} \quad (11)$$

in which $\eta_{\min} = P/(2\zeta_{\max}) = 2 \times 10^{-9} \text{ s}^{-1}$. (11) allows an isotropic tension in diverging flow until η reaches η_{\min} when it becomes and remains zero. Tensile stress is prohibited by taking the further limit $\eta_{\min} \rightarrow 0$, when $\zeta_{\max} \rightarrow \infty$, and (11) reduces to

$$N_{ij} = -PH(-\eta)\delta_{ij} \quad (12)$$

It is found that the abrupt cut-off by the Heaviside function in (12) leads to an ill-conditioned problem which is generally unstable, but the smooth transitions through $\eta = 0$ and $\eta = \eta_{\min}$ in (11) removes the numerical ill-conditioning. Note that the normality condition to the yield line $N_1 = N_2$, becomes an incompressibility condition $D_1 + D_2 = 0$.

Next, consider rheologies derived from the Reiner–Rivlin viscous fluid law, which in two dimensions has the general form

$$N_{ij} = -\Phi_0 \delta_{ij} + \Phi_1 \hat{D}_{ij} \quad (13)$$

The response coefficients Φ_0 and Φ_1 are functions of the state variables A, h and the strain-rate invariants η, γ . The functional forms of Φ_0 and Φ_1 should be chosen so that the qualitative behaviour of the stress is in agreement with observed behaviour, but as yet there are no established forms. The simplest possible constitutive relation corresponds to that for a linearly viscous fluid with equal constant bulk and shear viscosities, $\zeta = \mu$, which is obtained by taking $\Phi_0 = -\zeta\eta = -\eta\Phi_1/2$, where $\Phi_1 = \mu$. Hence, if a linearly viscous fluid relation is assumed for converging flow with no stress in diverging flow, then

$$N_{ij} = \Phi_1 D_{ij} H(-\eta) \quad (14)$$

For the shear viscosity Φ_1 we adopt the thickness and area fraction dependence

$$\Phi_1 = h A f(A) v \quad (15)$$

in which v is a viscosity scale parameter, which corresponds to the previous strength factor dependence. While the constitutive relation (14) does not contain many of the features generally regarded as essential for realistic ice models, a single viscosity constant offers the most simple model to assess a viscous response, and in particular, the instability caused by abrupt cut-off of tensile stress. It will be used only to point out important features.

A second model based on the Reiner–Rivlin law (13) which will be considered, is that proposed by Overland and Pease.¹¹ In this rheology, which will be referred to as the OP-rheology, the isotropic stress depends only on the state variables h and A while the deviatoric stress depends also on the shear strain-rate invariant γ . The specific forms for the functions Φ_0 and Φ_1 are

$$\Phi_0 = h P(A, h) H(-\eta), \quad \Phi_1 = \sqrt{2D} \frac{\Phi_0}{\gamma_0 + \gamma} H(-\eta) \quad (16)$$

in which $P(A, h)$ is defined in (10) and D, γ_0 are empirical constants. The parameter D is a coefficient of internal friction, while γ_0 is a shear strain-rate at which the viscosity decrease with γ becomes significant. An important difference between the OP-rheology and all other rheologies considered in this paper is the quadratic dependence of the isotropic stress Φ_0 on the ice thickness h [recall that $P(A, h)$ is a linear function of h].

The assumption of zero stress in diverging flow, evident in (12), (14) and (16) through the factor $H(-\eta)$, and typically applied by numerical cut-off in applications with the viscous-plastic model (5), is the common practice. From a mathematical point of view, switching off the stress abruptly in divergence leads to an ill-posed problem: an arbitrarily small change in the divergence rate through zero leads to a large change in the response of the system. Not surprisingly, this leads to an ill-conditioned numerical system of equations with very small changes in variables leading to large changes in response, which has commonly been rectified by introducing an artificial numerical viscosity with consequent uncertainties. Examples of this ill-conditioned behaviour

will be given in Section 5. Recall, however, that our model of a floating ice pack, which consists of a multitude of floes interspersed with regions of open water, is a continuum. Divergence in a continuum problem implies divergence in a mean sense of some ensemble of floes. A mean divergence of an ensemble of ice floes does not prevent inter-floe interactions on a local scale. Hence, while on a local scale a purely diverging flow field prevents the interaction of individual floes, divergence in some mean sense does not prevent interactions. The idea that stresses should switch off abruptly in divergence results from the extension of this local response to determine the mean response of the continuum, which is the most simple interpretation. Continuing a given constitutive relation for converging flow into diverging flow, and allowing tensile stresses to develop, may not reflect the actual mean response, but in the absence of any clear alternative, this continuation approach will be adopted with the above models to determine which allows a stable solution without an artificial numerical viscosity. It may further be argued, that in some situations, ignoring the Heaviside function does not lead to significant tensile stress. In a diverging flow field, the evolution equations (2) and (3) lead to a decrease of the area fraction. This property, together with the fact that the ice strength and viscous functions Φ_0 and Φ_1 decrease rapidly for decreasing A when A is near unity, imply that the predicted tensile stress decreases rapidly. For example, taking the ice strength function $f(A)$ to be the exponential function postulated by Hibler,¹ starting from an area fraction close to unity, the ice strength and viscosity reduce by a factor of 3 with a reduction in the area fraction of just 5 per cent. A 10 per cent decrease in the area fraction leads to an 8 fold decrease in the ice strength and the viscosity. Of course there may be a large short-term tensile stress, and this rapid decrease does not follow if the diverging flow starts from a lower area fraction.

4. NUMERICAL SOLUTION

In order to solve equations (1)–(3), where the stress–strain relation is given by one of the four rheologies outlined in the previous section, a suitable set of boundary conditions is required. It is assumed that the boundary $\partial\Omega(t)$ of some time-dependent domain $\Omega(t)$ is divided into two separate parts $\partial\Omega_1$ and $\partial\Omega_2$ ($\partial\Omega = \partial\Omega_1 \cup \partial\Omega_2$). On the boundary $\partial\Omega_1$ it is assumed that the ice is bonded so that the normal velocity is zero, and that either there is no-slip, i.e.

$$\mathbf{v} = 0, \quad \text{for } (x, y) \in \partial\Omega_1 \quad (17)$$

or that $\partial\Omega_1$ is a free-slip boundary, giving

$$\left. \begin{array}{l} v_n = \mathbf{v} \cdot \mathbf{n} = 0 \\ N_\tau = 0 \end{array} \right\} \quad \text{for } (x, y) \in \partial\Omega_1 \quad (18)$$

In the above equations $N_\tau = \sum_{i,j=1}^2 N_{ij} n_i t_j$ denotes the tangential stress and \mathbf{n}, \mathbf{t} denote unit normal and tangential vectors on the boundary $\partial\Omega$. The boundary $\partial\Omega_2$ is assumed to be a stress-free boundary giving

$$\left. \begin{array}{l} N_n = 0 \\ N_\tau = 0 \end{array} \right\} \quad \text{for } (x, y) \in \partial\Omega_2 \quad (19)$$

with $N_n = \sum_{i,j=1}^2 N_{ij} n_i n_j$ denoting the normal stress. Note that the stress-free conditions on the boundary $\partial\Omega_2$ indicate that the shape of this boundary deforms under the action of deformations inside Ω . Hence, the shape of the domain is a function of time.

Equations (1)–(3) subject to the boundary conditions (17)–(19) are solved here by a finite-element method.[§] To this end a variational formulation of the governing equations is required. This is done in the usual way by multiplying equations (1)–(3) by sufficiently smooth test functions, \mathbf{w} and q say, and using partial integration to reduce the order of differentiation; see, e.g. Cuvelier *et al.*²¹. After some algebra the variational formulation of equations (1)–(3) is reduced to finding \mathbf{v} , h and $A \in \Omega$ such that the following equations are satisfied for all \mathbf{w} , $q \in \Omega$:

$$\left\{ \begin{aligned} \int_{\Omega} \rho h \left(\frac{\partial \mathbf{v}}{\partial t} + (\mathbf{v} \cdot \nabla) \mathbf{v} \right) \cdot \mathbf{w} \, d\mathbf{x} + a(\mathbf{v}, \mathbf{w}) &= \int_{\Omega} (\mathbf{f}_T + \mathbf{f}_B) \cdot \mathbf{w} \, d\mathbf{x} \\ \int_{\Omega} \left(\frac{\partial A}{\partial t} + (\mathbf{v} \cdot \nabla) A \right) q \, d\mathbf{x} + \int_{\Omega} A \nabla \cdot \mathbf{v} (1 - \mathcal{R}) q \, d\mathbf{x} &= 0 \\ \int_{\Omega} \left(\frac{\partial h}{\partial t} + (\mathbf{v} \cdot \nabla) h \right) q \, d\mathbf{x} + \int_{\Omega} h \nabla \cdot \mathbf{v} \mathcal{R} q \, d\mathbf{x} &= 0 \end{aligned} \right. \quad (20)$$

The functional $a(\mathbf{v}, \mathbf{w})$ in the first of the above equations, defined as

$$a(\mathbf{v}, \mathbf{w}) = \frac{1}{2} \sum_{i,j=1}^2 \int_{\Omega} N_{ij} \left(\frac{\partial w_j}{\partial x_i} + \frac{\partial w_i}{\partial x_j} \right) d\mathbf{x} \quad (21)$$

is a measure of the deformation energy stored in the system. Note that after the application of partial integration there is no boundary integral left in the first of the equations in (20). This is due to the fact that with the boundary conditions as given, all the terms in the boundary integral vanish.

In order to obtain a discrete set of equations, the velocity field together with the area fraction and the ice thickness are approximated by a finite sum of interpolating polynomials. In particular,

$$\begin{aligned} v_i(\mathbf{x}, t) &= \sum_{j=1}^N v_{ij}(t) \phi_j(\mathbf{x}) \\ A(\mathbf{x}, t) &= \sum_{j=1}^N A_j(t) \psi_j(\mathbf{x}) \\ h(\mathbf{x}, t) &= \sum_{j=1}^N h_j(t) \psi_j(\mathbf{x}) \end{aligned} \quad (22)$$

The domain Ω is divided into triangular elements and on each element the functions ϕ_j and ψ_j are taken to be piecewise linear interpolating polynomials. The system of equations which results after the discretization procedure has been applied to (20) is of the form

$$\mathbf{M}(\mathbf{u}) \frac{\partial \mathbf{u}}{\partial t} + \mathbf{C}(\mathbf{u}) \mathbf{u} + \mathbf{S}(\mathbf{u}) \mathbf{u} = \mathbf{f}(\mathbf{u}), \mathbf{u}^T = (\hat{\mathbf{v}}_x, \hat{\mathbf{v}}_y, \hat{\mathbf{A}}, \hat{\mathbf{h}}) \quad (23)$$

[§] The finite-element program SEPRAN developed by A. Segal in the Mathematics Department of Delft University of Technology has been used

In the above equation $\hat{\mathbf{v}}_x, \hat{\mathbf{v}}_y, \hat{\mathbf{A}}, \hat{\mathbf{h}}$ denote vectors of function values at the nodal points. The mass matrix \mathbf{M} is related to the time-derivative terms in (20), the matrix \mathbf{C} refers to the convective terms, the stiffness matrix \mathbf{S} refers to the contribution from the energy functional $a(\mathbf{v}, \mathbf{w})$ and the terms containing the ridging function \mathcal{R} , and finally, the vector \mathbf{f} refers to the external forcing due to ocean drag and wind stress. Note that the matrices \mathbf{M} , \mathbf{C} and \mathbf{S} are functions of the nodal point values and, hence, the system of equations (23) is non-linear.

To integrate (23) in time the so-called θ -method is used. For a system of ordinary differential equations of the form

$$\frac{\partial \mathbf{u}}{\partial t} = \mathbf{F}(\mathbf{u}, t) \quad (24)$$

the θ -method reads

$$\frac{\mathbf{u}^{n+1} - \mathbf{u}^n}{\Delta t} = \theta \mathbf{F}(\mathbf{u}^{n+1}, t^{n+1}) + (1 - \theta) \mathbf{F}(\mathbf{u}^n, t^n), \quad 0 \leq \theta \leq 1 \quad (25)$$

in which the superscript n denotes the n th time level. Special cases of the θ -method are: $\theta = 0$, explicit Euler; $\theta = 1/2$, Crank–Nicolson; $\theta = 1$, implicit Euler. It is simple to show that the θ -method is unconditionally stable for $\theta > 0.5$. In all calculations the value $\theta = 0.6$ is taken, which ensures unconditional stability and has the added benefit that the discretisation error is almost second-order (the global error is $O(\Delta t^2)$ for $\theta = 1/2$). Application of the θ -method to the system of equations (23) yields a non-linear systems of equations for \mathbf{u}^{n+1} . In order to avoid iterations at each time step it is assumed that the matrices and the forcing vector do not change rapidly with time and may therefore be regarded as constant during one complete time step. This yields the following system of equations to be solved at each time step

$$[\mathbf{M}^n + \theta \Delta t (\mathbf{C}^n + \mathbf{S}^n)] \mathbf{u}^{n+1} = [\mathbf{M}^n - (1 - \theta) \Delta t (\mathbf{C}^n + \mathbf{S}^n)] \mathbf{u}^n + \Delta t \mathbf{f}^n \quad (26)$$

The approximation that the matrices and the forcing vector are constant during one time step of course affects the accuracy of the integration scheme. In the worst case, the global error is $O(\Delta t)$ even with $\theta = \frac{1}{2}$. However, calculations show that in particular for the mass and the stiffness matrices the simplifying assumption of constant matrices is certainly justified. For this reason it is expected that the accuracy of the integration routine is higher than $O(\Delta t)$.

Since it has been assumed that the boundary $\partial\Omega_2$ is a stress-free boundary, the shape of this boundary (and hence, the shape of the whole domain Ω) will deform during the time integration. In order to deal with the moving boundary the following approach is adopted. On a given grid the velocity field is calculated using (26). Given the velocity field, the nodal points on the boundary are relocated simply by moving a nodal point with position vector \mathbf{x}^n at time t^n to a new position at \mathbf{x}^{n+1} via

$$\mathbf{x}^{n+1} = \mathbf{x}^n + \Delta t \mathbf{v}^n$$

Once the deformation of the free boundary is known, a new mesh is calculated such that changes in the mesh reflect the topological changes of the free boundary. The values of the velocity components, the thickness and the area fraction at the new nodal positions are calculated simply by linear interpolation of the values determined at time t^{n+1} at the former nodes.

5. RESULTS

To specify the model problem to be studied, consider a Cartesian co-ordinate system with co-ordinates denoted by (x, y) . The initial ice cover is assumed to be a rectangular slab of 25×50 km. The cover is at rest at $t = 0$, and in all but the first set of simulations in which the effect of the Heaviside function is investigated, the initial ice cover has a uniform area fraction $A_0 = 0.9$ and ice thickness $h_0 = 2$ m. The boundaries $y = 0$, $x \in [0, 25 \text{ km}]$ and $x = 0$, $y \in [0, 50 \text{ km}]$ are the solid boundaries denoted by $\partial\Omega_1$ on which the conditions (17) or (18) hold. On the stress-free boundary $\partial\Omega_2$, initially situated at $x = 25 \text{ km}$, $y \in [0, 50 \text{ km}]$ and $y = 50 \text{ km}$, $x \in [0, 25 \text{ km}]$ the conditions (19) hold. It is assumed that at $t = 0$ a uniform wind stress is applied in the direction of the negative y -axis, giving

$$\mathbf{f}_T = (0, -C_a) \quad (27)$$

in which C_a is the atmospheric drag coefficient. A linear drag relation is assumed for the traction between the base of the ice cover and the underlying water, so that

$$\mathbf{f}_B = -\rho_w C_w \mathbf{v} \quad (28)$$

with ρ_w denoting the water density and C_w the water drag coefficient. Note that C_a and C_w conventionally have different dimensions; see Table I. The alternative commonly assumed quadratic relations do not change the structure of the equations, and would not influence the numerical stability. For the ridging function $r(A, h)$ as defined in (4) we take

$$r(A, h) = Af(A) \quad (29)$$

with $f(A)$ as defined in (10). Note that this choice of $r(A, h)$ satisfies the required conditions in the limits $A \rightarrow 0$, $A \rightarrow 1$. Choosing the ridging function to be of the same form as the function characterising the ice strength is motivated simply by the fact that the ice strength is inherently linked to ridging effects. While more exotic forms of ridging functions are easy to construct (see, e.g. Reference 4), they would not influence the stability nor the distinction between the rheology effects. The parameters used in the numerical simulation are listed in Table 1. The initial finite-element mesh is plotted in Figure 1 and the boundaries $\partial\Omega_1$ and $\partial\Omega_2$ are indicated. Note that an element size decreasing towards the solid boundaries has been adopted, since, as will become apparent shortly, boundary-layer-like regions may develop near a solid boundary.

In the first set of numerical simulations, the role of the Heaviside function in the constitutive relation will be investigated. In order to avoid complicated rheological effects, the simple linear viscous relation as given in (14) is used. Free-slip boundary conditions as given by (18) are prescribed on $\partial\Omega_1$, but further numerical tests have shown that the qualitative behaviour resulting from the presence of the Heaviside function was independent of the type of boundary conditions applied. The initial ice thickness is taken to be $h_0 = 2$ m, and the initial area fraction is taken to be $A_0(\mathbf{x}) = 1 - 1.2x \times 10^{-5}$ where x is in metres, which means that the area fraction changes from $A_0 = 1$ on the solid boundary to $A_0 = 0.7$ on the free boundary. An example of what is typically observed in calculations in which the Heaviside function is applied, is shown in Figures 2(a)–2(c), 8 h after the simulation started. The velocity vector field shown in Figure 2(a) shows a clear discontinuity near the upper edge of the ice cover. When plots of the area fraction A and the divergence rate η are considered, it becomes clear that a crack-like feature has developed. The crack develops due to the transition from convergent to divergent flow near the upper edge of the ice cover. In the crack the area fraction decreases rapidly due to the strong divergence within the crack (cf. Figure 2(c)). At the time shown the calculation proceeded in

Table I. Values of parameters used in the numerical simulations

| | | |
|----------------------------------|---------------|---|
| <i>Initial conditions</i> | | |
| Initial ice thickness | h_0 | 2.0 m |
| Initial area fraction | A_0 | 0.9 |
| <i>Numerical parameters</i> | | |
| Time step | Δt | 0.02 h |
| Discretisation | | 600 triangular elements |
| Total integration time | | 3 days |
| <i>Physical parameters</i> | | |
| Ice density | ρ | $0.918 \times 10^3 \text{ kg m}^{-3}$ |
| Water density | ρ_w | $1.02 \times 10^3 \text{ kg m}^{-3}$ |
| Ice strength parameter | P^* | $5 \times 10^3 \text{ kg m}^{-1} \text{ s}^{-2}$ |
| Strength-compactness coefficient | K | 15 |
| Atmospheric drag coefficient | C_a | $5.0 \times 10^{-2} \text{ kg m}^{-1} \text{ s}^{-2}$ |
| Water drag coefficient | C_w | $5.0 \times 10^{-4} \text{ m s}^{-1}$ |
| <i>Rheological parameters</i> | | |
| VP-rheology | e | 2 |
| | Δ_c | $2.0 \times 10^{-9} \text{ s}^{-1}$ |
| CF-rheology | η_{\min} | $2.0 \times 10^{-9} \text{ s}^{-1}$ |
| OP-rheology | D | 0.6 |
| | γ_0 | 1.0×10^{-5} and $1.0 \times 10^{-9} \text{ s}^{-1}$ |
| Newtonian fluid | ν | $1.0 \times 10^9 \text{ kg m}^{-1} \text{ s}^{-1}$ |

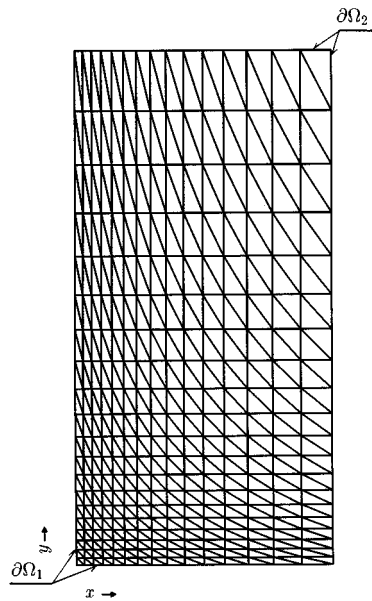


Figure 1. The finite-element mesh at the start of the calculation

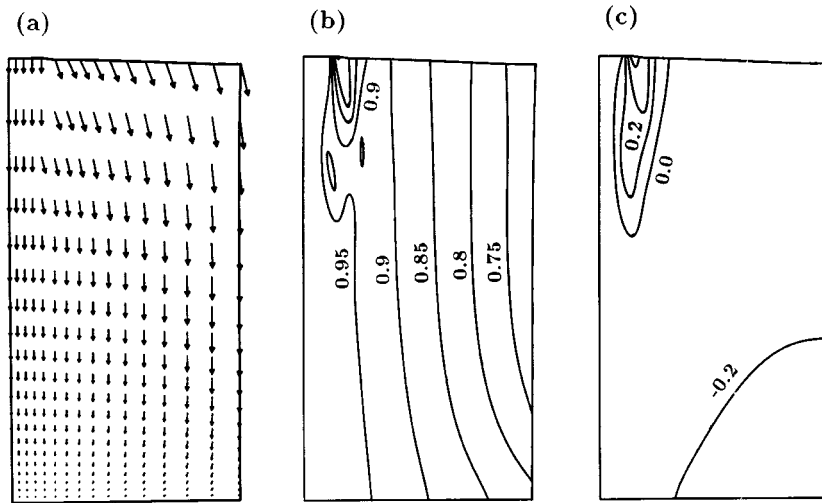


Figure 2. Linearly viscous fluid rheology. Free-slip conditions on $\partial\Omega_1$. Plots (a) the velocity vector field, (b) the area fraction A and (c) the velocity divergence η in units 10^{-5} s^{-1} , after 8 h

a stable manner, but usually the calculation becomes unstable a few hours after the crack appears. The reason for this unstable behaviour is the following. With the triangular elements used in the present calculation there are three nodal points associated with each element. Hence, if in one element the flow field is divergent so that the Heaviside function forces the stress to switch off, the effect of this switching-off is felt in all three nodes of the element. This leads to a reduction in the stress in all elements surrounding the element under consideration. Hence, the influence of the Heaviside function spreads out. Numerically it is found that the whole flow field is eventually affected by the crack which started as a local feature. Often the calculation becomes unstable with checker-board like patterns developing, indicating alternating switching-on and switching-off of the Heaviside function. Only by resorting to excessive artificial damping could this instability be suppressed, but then the solution is also distorted. The same situation will arise with other elements, and also arises with staggered grids in finite-difference calculations. Repeating the simulations with the other rheologies with the Heaviside function present shows the same instability. The subsequent simulations discard the Heaviside function, allowing tensile stress, governed by the same constitutive relation applied to positive η , to arise in diverging flow regions.

Free-slip boundary conditions

The dynamics of the ice cover was found to be significantly altered depending on whether free-slip or no-slip conditions were imposed on the solid boundary $\partial\Omega_1$. For this reason the behaviour of the ice cover for the different rheologies is investigated separately for the two different boundary conditions. In this section it is assumed that the boundary condition on the solid boundary $\partial\Omega_1$ is the free-slip condition (18). The first rheology to be investigated is the viscous-plastic rheology without the tensile stress cut-off. In Figures 3(a)–3(c) plots of the velocity field vectors after 1, 2 and 3 days, respectively, are shown, and in Figures 3(d)–3(f) the area fraction A , the velocity divergence η , and the shear strain-rate invariant γ after 1 day are shown. In

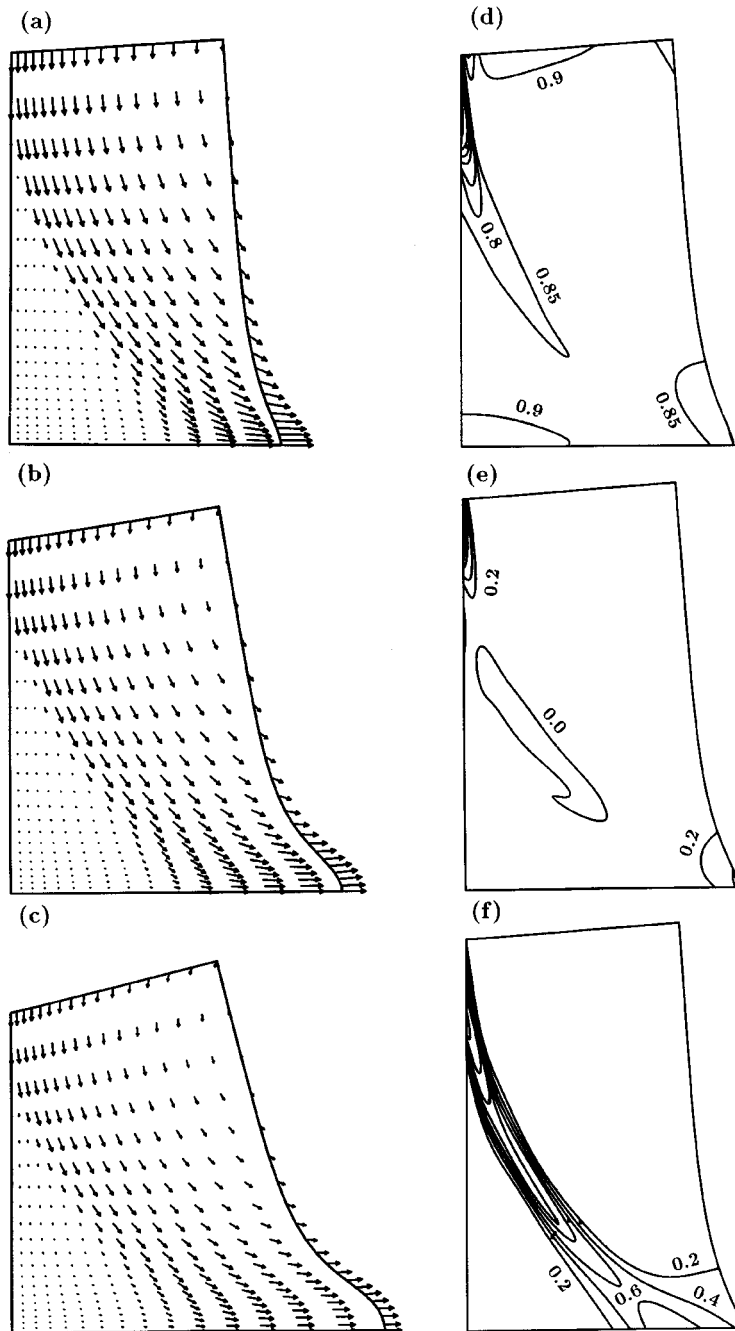


Figure 3. Viscous-plastic rheology. Free-slip conditions on $\partial\Omega_1$. Plots of the velocity vector field (a) after 1 day, (b) after 2 days, (c) after 3 days. Contour plots (d) the area fraction A , (e) the velocity divergence η in units 10^{-5} s^{-1} , and (f) the shear strain-rate invariant γ in units 10^{-5} s^{-1} , after 1 day

accordance with expectations it is observed that as the ice is driven towards the solid boundary at $y = 0$, the area fraction near this boundary increases, but the largest changes in area fraction occur near the free boundary initially at $x = 25$ km, with the maximum change about 30 per cent (from 0.7 to 0.9). In contrast, changes in the ice thickness were less than 1 per cent. Close to the solid boundary towards which the ice cover is driven, it is observed that the domain has stretched significantly. Figure 3(f) shows the concentrated region of high shear strain-rate invariant γ , which is characteristic of rheologies in which a yield stress is invoked, and reflects the rapid change in velocity shown in Figures 3(a)–3(c). In regions where the stress is small, that is smaller than the yield stress, the cover behaves as a highly viscous medium which undergoes only slight deformations.

Next, consider the behaviour of the cavitating fluid model (12) without the Heaviside function. Figures 4(a)–4(c) illustrate the evolution of the shape of the ice cover and the velocity field in a three-day period, and Figures 4(d)–4(f) the distributions of the area fraction A , the velocity divergence η , and the shearing γ after 1 day. One clear difference between the CF-rheology and the VP-rheology is the marked increase in the deformation of the ice cover with the CF-rheology as compared with the VP-rheology. This change should not be surprising given the fact that the CF-rheology has no shear strength: the ice cover deforms easily under the action of external forces. A further difference between the CF-rheology and the VP-rheology is that in the case of the CF-rheology the variation of the area fraction is significantly less than with the VP-rheology. The very small changes in the ice thickness (not shown) and the area fraction are indicative of small values of η . Small convergence (or divergence) rates are, in turn, the result of the absence of shear stresses in the cavitating fluid model. Namely, large convergence rates lead to large gradients in the isotropic stress. However, such gradients can be sustained for any length of time only when the deviatoric stress gradients can balance the isotropic stress gradients. Since the deviatoric stress is (almost) absent in the CF-rheology, gradients in the isotropic stress cannot be sustained. Instead, gradients are translated into large domain deformations while the ice thickness and the area fraction change only slightly. Applying the law (12) with the Heaviside function retained leads to instability as reported earlier, but the law (11) allows stable solutions.

Results obtained using the OP-rheology (16) without the Heaviside function, and with $\gamma_0 = 10^{-5} \text{ s}^{-1}$ are presented in Figure 5. When the evolution of the domain is compared with that observed for the VP- and the CF-rheologies, it is seen that the domain deformation for the OP-rheology with γ_0 relatively large is very similar to that for the CF-rheology. As in the CF-rheology, the variation in the ice thickness during the simulation is very small in the case of the OP-rheology. This is in stark contrast to the variation in the area fraction. In Figure 5(b) it can be observed that the area fraction decreases significantly towards the free boundary of the domain. This is not observed in either the VP-rheology, Figure 3(d), or in the CF-rheology, Figure 4(d).

Finally, consider the response of the ice cover in the case of the OP-rheology when $\gamma_0 = 10^{-9} \text{ s}^{-1}$. In the limit $\gamma \rightarrow 0$, this value of γ_0 yields a shear viscosity which is of the same order of magnitude as the maximum viscosity in Hibler's¹ viscous-plastic rheology. Since $\gamma = 0$ at $t = 0$, the smaller value of γ_0 indicates a larger value of the viscosity during the initial stages of the motion. For this reason it is anticipated that the deformation of the ice cover in the initial stage is less than that observed for the case with $\gamma_0 = 10^{-5} \text{ s}^{-1}$. In Figures 6(a)–6(d) the velocity vector field, and contour plots of the area fraction A , the velocity divergence η , and the shear strain-rate invariant γ , respectively, after 1 day are shown. The evolution of the area fraction and the ice thickness did not change qualitatively from the case in which $\gamma_0 = 10^{-5} \text{ s}^{-1}$: the area fraction decreases towards the free boundary. When Figures 5 and 6 are compared, it is immediately

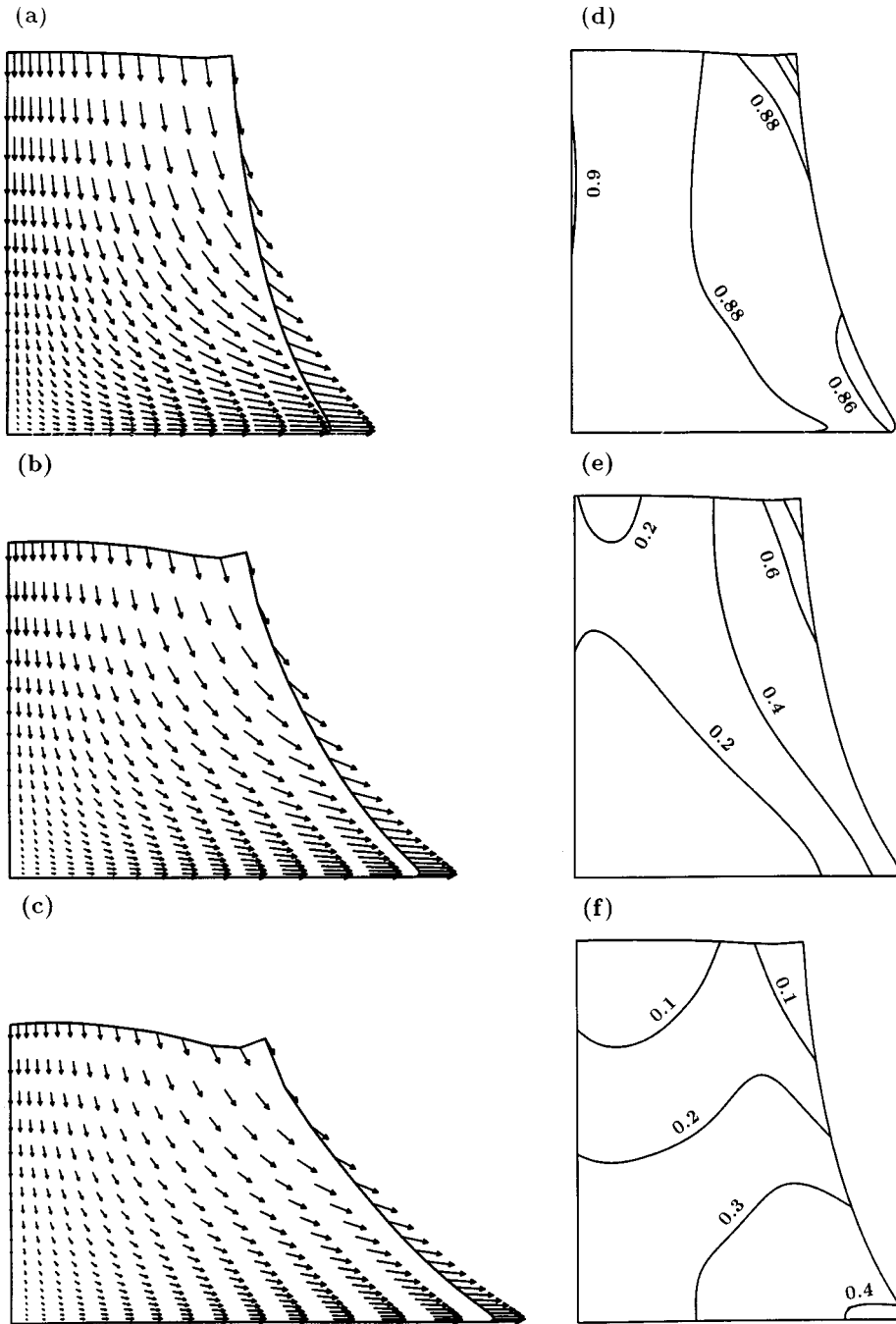


Figure 4. Cavitating fluid rheology. Free-slip conditions on $\partial\Omega_1$. Plots of the velocity vector field (a) after 1 day, (b) after 2 days, (c) after 3 days. Contour plots (d) the area fraction A , (e) the velocity divergence η in units 10^{-6}s^{-1} , and (f) the shear strain-rate invariant γ in units 10^{-6}s^{-1} , after 1 day

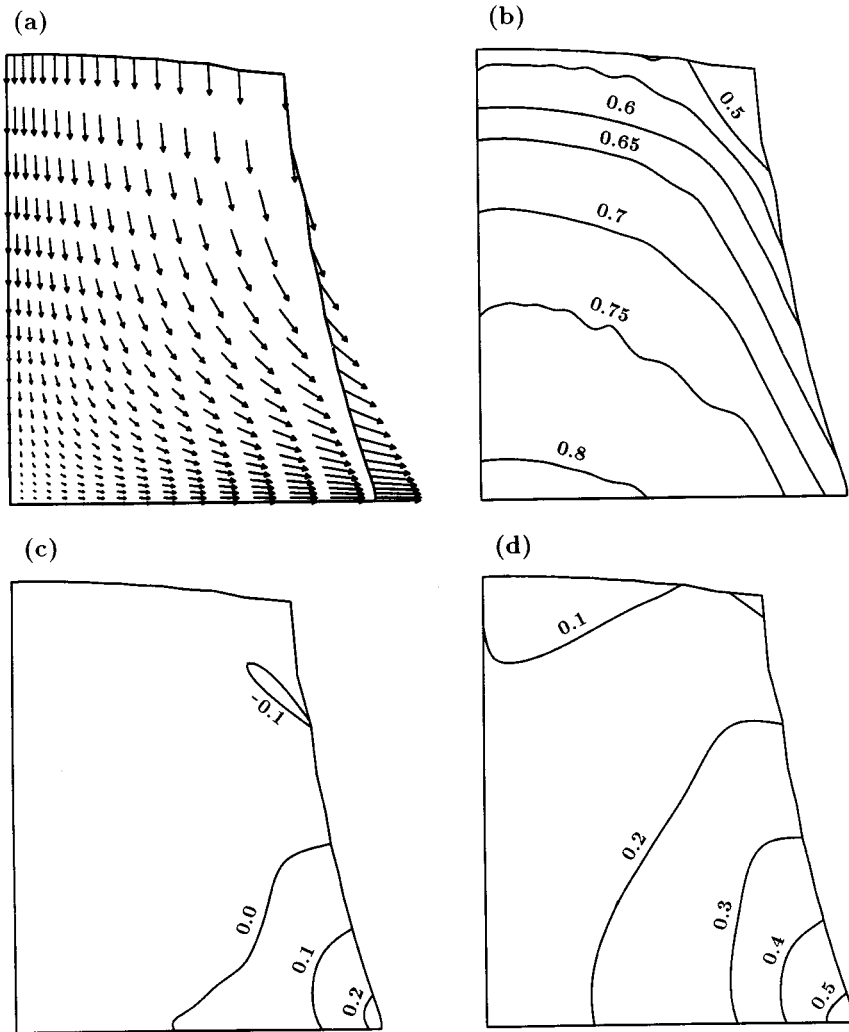


Figure 5. Overland-Pease rheology with $\gamma_0 = 10^{-5} \text{ s}^{-1}$. Free-slip conditions on $\partial\Omega_1$. Plots (a) the velocity vector field, (b) the area fraction A , (c) the velocity divergence η in units 10^{-5} s^{-1} , and (d) the shear strain-rate invariant γ in units 10^{-5} s^{-1} , after 1 day

apparent that decreasing γ_0 leads to a drastic decrease in the deformation of the domain. While with $\gamma_0 = 10^{-5} \text{ s}^{-1}$ the rectangular shape of the ice domain has all but disappeared after 1 day, with $\gamma_0 = 10^{-9} \text{ s}^{-1}$ the rectangular shape, albeit distorted, is still clearly present. Comparison of Figures 6(d) and 3(f) illustrating the shear strain-rate invariant γ shows that the OP-rheology with relatively small γ_0 causes a highly concentrated region of shearing similar to that caused by the viscous-plastic rheology.

When the direction of the vectors in the velocity plot in Figure 6 is considered, it is clear that a characteristic direction is associated with the OP-rheology. This direction is related to the

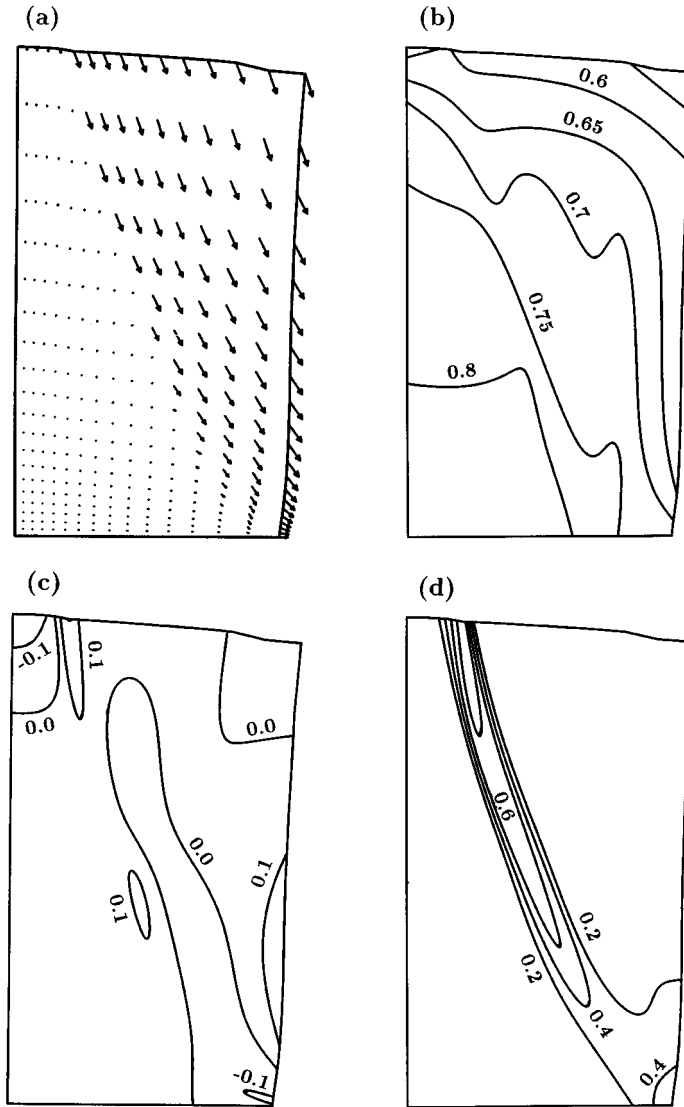


Figure 6. Overland-Pease rheology with $\gamma_0 = 10^{-9} \text{ s}^{-1}$. Free-slip conditions on $\partial\Omega_1$. Plots (a) the velocity vector field, (b) the area fraction A , (c) the velocity divergence η in units 10^{-5} s^{-1} , and (d) the shear strain-rate invariant γ in units 10^{-5} s^{-1} , after 1 day

parameter D which is the coefficient of internal friction. In fact, the inclination of slip-lines (lines along which failure in the ice pack occurs) with the horizontal is given by

$$\phi = \frac{\pi}{2} - \tan^{-1} D \quad (30)$$

The parameter value $D = 0.6$ corresponds to $\phi = \pi/3$ which is in good agreement with the observed characteristic direction in Figures 6.

No-slip boundary conditions

Now, consider the case in which the no-slip conditions (17) are specified on the boundary $\partial\Omega_1$. The first rheology to be considered is the VP-rheology. Figures 7(a)–7(d) show plots of the velocity vector field and contour plots of the area fraction, velocity divergence and shear strain-rate invariant after 1 day. When Figure 7 is compared with the free-slip case shown in Figure 3, the large influence of the boundary conditions is immediately apparent. The most dramatic feature resulting from the application of the no-slip conditions is the cracking behaviour adjacent to the solid boundary $x = 0$, at the top edge $y = 50$ km, where the area fraction

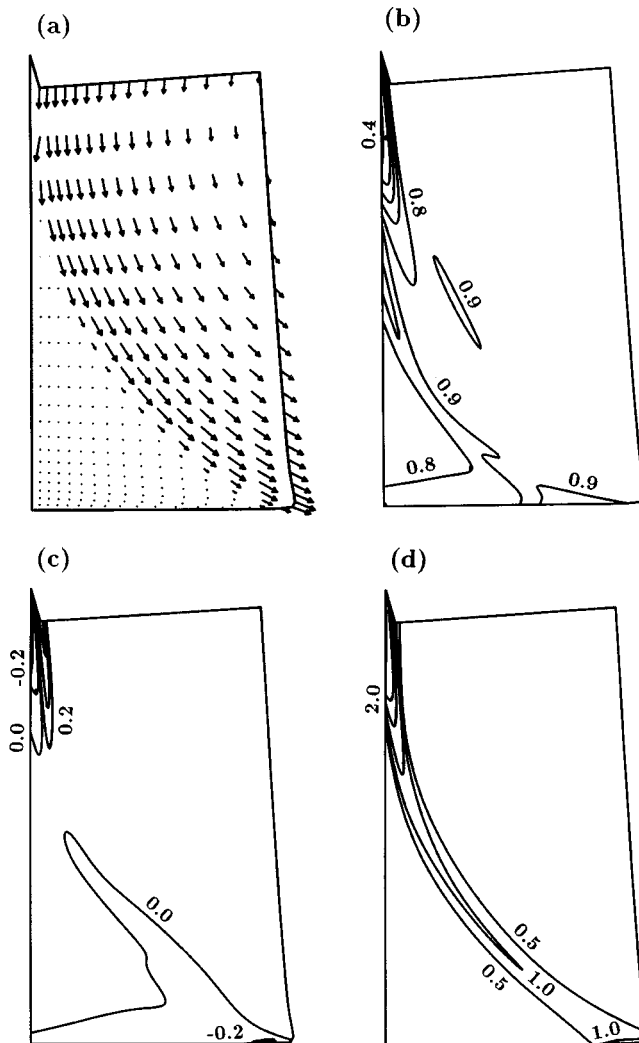


Figure 7. Viscous-plastic rheology. No-slip conditions on $\partial\Omega_1$. Plots (a) the velocity vector field, (b) the area fraction A , (c) the velocity divergence η in units 10^{-5} s^{-1} , and (d) the shear strain-rate invariant γ in units 10^{-5} s^{-1} , after 1 day

decreases rapidly. In fact, the reduction of the area fraction precedes the formation of the crack. This observation adds some weight to the argument in Section 3 concerning the use of the Heaviside function. Clearly there is no need for a procedure to switch-off stresses in divergence: divergence leads to a decrease in the area fraction with a corresponding rapid decrease in the ice strength. However, this crack development leads to a severe distortion of the numerical mesh which is also the onset of a numerical instability, distinct from that caused by an abrupt stress cut-off.

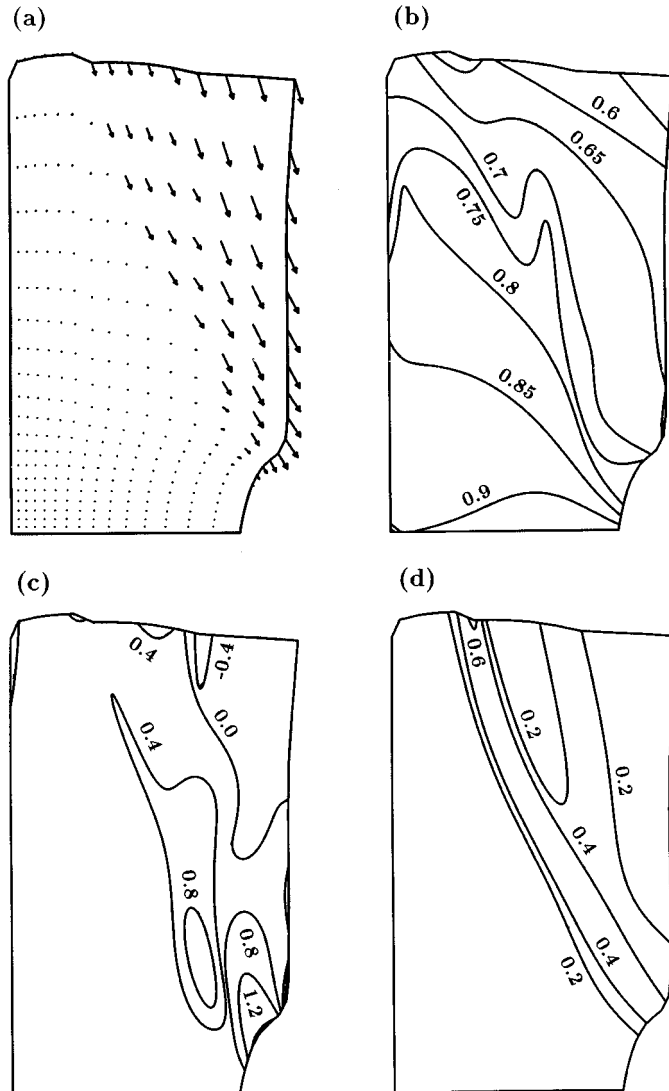


Figure 8. Overland-Pease rheology with $\gamma_0 = 10^{-9} \text{ s}^{-1}$. No-slip conditions on $\partial\Omega_1$. Plots (a) the velocity vector field, (b) the area fraction A , (c) the velocity divergence η in units 10^{-5} s^{-1} , and (d) the shear strain-rate invariant γ in units 10^{-5} s^{-1} , after 1 day

Finally, consider the dynamics of the ice cover in the case of the OP-rheology when no-slip conditions are prescribed on the solid boundary, and take $\gamma_0 = 10^{-9} \text{ s}^{-1}$. Plots of the velocity vector field, area fraction A , velocity divergence η , and shear strain-rate invariant γ are shown in Figure 8. A comparison with Figure 5 shows once more the large effect of the boundary conditions on the evolution of the ice cover. As before, the presence of a narrow region of rapid velocity change is evident.

6. CONCLUSIONS

The abrupt cut-off of tensile stress in diverging flow, without artificial numerical diffusion, has been shown to lead to numerical instability for the typical ice rheologies used in ice pack dynamics simulations. The characteristics of three different common rheologies for large-scale ice covers, namely the viscous-plastic rheology, the cavitating fluid model and a non-linearly viscous fluid model, have been compared when abrupt cut-off of tensile stress is not applied. A special feature of the ice pack considered is the presence of an extensive free boundary which allows the domain to deform significantly under the action of external forces, and the effects of the different rheologies on the domain deformation have been compared. In addition, the effect of the fixed boundary conditions on the evolution of the ice cover has been examined. The equations were discretised using a finite-element procedure, and an implicit time-stepping scheme was used which ensured unconditional stability during the time integration. No artificial diffusive terms were used in any of the models.

As expected, the rheology has a large effect on the deformation of the free boundary. It is found that the free boundary is very well-suited to display one of the main characteristics of the viscous-plastic rheology, namely, the yield stress behaviour. Typically, it is observed that the free boundary deforms significantly only when yielding occurs elsewhere in the domain. This is in stark contrast to the behaviour observed with the cavitating fluid model. Since the cavitating fluid model eliminates the shear strength of the ice cover, the entire domain deforms rapidly and easily for this rheology. The non-linearly viscous fluid model can lead to large domain deformations provided the viscosity is sufficiently small or sufficiently large shear rates are generated to lower the shear viscosity.

The evolution of the ice cover for all rheologies is very sensitive to the boundary conditions imposed on the solid boundary. In general, it was found that the imposition of no-slip boundary conditions inhibited the deformation of the domain. However, the presence of no-slip boundary conditions can lead to large shear rates near the solid boundaries. In the case of the viscous-plastic rheology it was found that the increased shear leads to the development of crack-like features adjacent to the solid boundary, and a severe distortion of the numerical mesh which causes instability.

A referee's report offered constructive comments and raised new questions. It was pointed out that ice-ocean models, commonly finite difference models, necessarily use coarse grids because of the size of the three-dimensional domains. Our two-dimensional description of the ice cover has used sufficiently fine grids to capture the spatial variations which arise in high-shear zones, and even then instabilities arise (without artificial damping) during extended time-stepping. Perhaps a coarse mesh would provide more smoothing, and stability, but this was not investigated since important features of the spatial response would then be lost. It would be convenient if tractable coupling of ocean and ice dynamics could accommodate coarse horizontal resolution in the ocean while retaining finer resolution in the ice cover. However, since coupling is through a drag

relation involving tangential tractions and velocities in both ocean and ice at their interface, rapid spatial changes in the ice must be reflected in the ocean variations. This important question can only be addressed by a specific substantial numerical investigation, not addressed in this paper.

We adopted two forms of boundary conditions for illustrations: no-slip with tangential velocity zero, and free-slip with tangential traction zero, but both with normal velocity zero, representing bonding between the coast and ice cover. No-slip and bonding reflects ice frozen onto the coast, but free-slip and bonding is artificial, adopted simply to compare two tangential extremes. Free-slip is accompanied by zero normal velocity if the local ice motion is towards the coast, but otherwise the ice boundary could move off the coast, giving rise to a more complicated free-boundary problem, again not addressed in this paper.

The choice between different ice rheologies is still an open question—which best predicts flow features in accord with observation. The main contenders must be the established Hibler viscous-plastic model and an alternative non-linearly viscous model which avoids the disjoint flow regimes. Further studies²² improving stability by a material co-ordinate formulation and implicit time-stepping also incorporate this comparison.

New boundary-value problems were suggested to investigate explicitly the effects of rheology on an idealised flow, and to model marginal ice-zone features and an ice bridge, which will be of interest in further studies.

ACKNOWLEDGEMENTS

The authors would like to thank Dr. J. M. N. T. Gray for constructive discussions during the course of this work, and NERC for support of the project.

REFERENCES

1. W. D. Hibler, 'A dynamic thermodynamic sea ice model', *J. Phys. Ocean.* **9**, 815–845 (1979).
2. A. S. Thorndike, D. A. Rothrock, G. A. Maykut and R. Colony, 'The thickness distribution of sea ice', *J. Geophys. Res.*, **80**, 4501–4513 (1975).
3. G. M. Flato and W. D. Hibler, 'Ridging and strength in modelling the thickness distribution of Arctic sea ice', *J. Geophys. Res.* **100**, 18611–18626 (1995).
4. Y. Shinohara, 'A redistribution function applicable to a dynamic model of sea ice', *J. Geophys. Res.*, **95**, 13423–13431 (1990).
5. J. M. N. T. Gray and L. W. Morland, 'A two-dimensional model for the dynamics of sea ice', *Phil. Trans. Roy. Soc. Lond.* **A 347**, 219–290 (1994).
6. R. M. S. M. Schulkes, 'Asymptotic stability of the viscous-plastic ice rheology', *J. Phys. Ocean.* **26**, 279–283 (1996).
7. W. D. Hibler, 'A viscous sea ice law as a stochastic average of plasticity', *J. Geophys. Res.* **82**(27), 3932–3938 (1977).
8. D. A. Rothrock, 'The energetics of the plastic deformation of pack ice ridging', *J. Geophys. Res.*, **80**, 4514–4519 (1975).
9. G. M. Flato and W. D. Hibler, 'Modelling pack ice as a cavitating fluid', *J. Phys. Ocean.* **22**, 626–651 (1992).
10. R. B. Smith, 'A note on the constitutive law for sea ice', *J. Glac.* **29**(101), 191–195 (1983).
11. J. Overland and C. Pease, 'Modelling ice dynamics of coastal seas', *J. Geophys. Res.* **93**(C12), 15619–15637 (1988).
12. N. R. Thomson, J. F. Sykes and R. F. McKenna, 'Short term ice motion modelling with applications to the Beaufort Sea', *J. Geophys. Res.*, **93**(C6), 6819–6836 (1988).
13. N. R. Thomson and J. F. Sykes, 'Sensitivity and uncertainty analysis of a short term sea ice motion model', *J. Geophys. Res.*, **95**(C2), 1713–1739 (1990).
14. M. Leppäranta and W. D. Hibler, 'The role of plastic ice interaction in marginal ice zone dynamics', *J. Geophys. Res.* **90**(C6), 11899–11909 (1985).
15. C. F. Ip, W. D. Hibler and G. M. Flato, 'On effects of rheology on seasonal ice simulations', *Annals of Glaciology*, **15**, 17–25 (1991).
16. W. D. Hibler and C. F. Ip, 'The effect of sea ice rheology on Arctic buoy drift', in: J. P. Dempsey and Y. D. S. Rajapakse (eds.), *ASME AMD 207, Ice Mechanics*, pp. 255–263 (1995).
17. G. M. Flato, 'A Particle-in-cell sea-ice model', *Atmos-Ocean* **31**(3), 339–358 (1993).

18. J. M. N. T. Gray and P. D. Killworth, Stability of the viscous-plastic sea ice rheology, *J. Phys. Ocean.*, **25**, 971–978 (1995).
19. C. L. Parkinson and W. M. Washington, 'A large-scale numerical model of sea-ice', *J. Geophys. Res.*, **84**(C1), 311–337 (1979).
20. R. S. Pritchard, A. C. Mueller, D. J. Hanzlick and Y.-S. Yang, 'Forecasting Bering Sea ice edge behaviour', *J. Geophys. Res.* **95**(C1), 775–788 (1990).
21. C. Cuvelier, A. Segal and A. A. Van Steenhoven, *Finite Element Methods and Navier–Stokes Equations*, Reidel, Dordrecht (1986).
22. L. W. Morland and R. Staroszczyk, 'A material co-ordinate treatment of the sea ice dynamics equations', *Proc. Roy. Soc. Lond.*, in press.